Molecular Therapy
Methods & Clinical Development
Original Article

Evidence of Accumulated Endothelial Progenitor Cells in the Lungs of Rats with Pulmonary Arterial Hypertension by ^{89}Zr-oxine PET Imaging

Yimin Liu,[1,4] Xin Zhao,[2,4] Jie Ding,[1] Yanjiang Xing,[2] Meijun Zhou,[2] Xuezhu Wang,[1] Wenjia Zhu,[1] Li Huo,[1] and Jun Yang[2,3]

[1]Department of Nuclear Medicine, Peking Union Medical College Hospital, Chinese Academy of Medical Sciences and Peking Union Medical College (CAMS & PUMC), Beijing 100730, China; [2]State Key Laboratory of Medical Molecular Biology, Department of Cell Biology, Institute of Basic Medical Sciences, Chinese Academy of Medical Sciences and School of Basic Medicine, Peking Union Medical College, Beijing 100730, China; [3]Department of Physiology, and Department of Cardiology of the Second Affiliated Hospital, Zhejiang University School of Medicine, Hangzhou 310058, Zhejiang, China

Endothelial progenitor cells (EPCs) play a major role in regulating pulmonary vascular remodeling during pulmonary arterial hypertension (PAH) development. Several preclinical and clinical trials of EPCs transplantation have been performed for the treatment of PAH. However, there is no reliable method to monitor real-time cell trafficking and quantify transplanted EPCs. Here in this paper we isolated EPCs from human peripheral blood, identified their functional integrity, and efficiently labeled the EPCs with ^{89}Zr-oxine and DiO. Labeled EPCs were injected into the tail vein of normal and PAH rats to be tracked *in vivo*. From the microPET/CT images, we found EPCs were distributed primarily in the lung at 1 h and then migrated to the liver and spleen. We could observe the 3,3′ dioctadecyloxacarbocyanine perchlorate (DiO)-labeled EPCs binding in the pulmonary vasculature by CellVizio confocal. The result of quantitative analysis revealed significantly higher accumulation of EPCs in the lungs of PAH rats than in those of healthy rats. The distribution and higher accumulation of EPCs in the lungs of PAH rats could help to evaluate the safety and provide evidence of effectiveness of EPC therapy.

INTRODUCTION

Pulmonary arterial hypertension (PAH), a severe condition with pulmonary vascular remodeling, results from a wide variety of etiologies.[1] Endothelial cells play a key role in maintaining the normal function of the pulmonary artery. The dysfunction of endothelial cells initiates the pathological process of pulmonary vascular diseases such as PAH.[2]

Endothelial progenitor cells (EPCs) were reported to be distributed mainly in the bone marrow and peripheral circulation system and to accumulate in the lesion area to function under pathological conditions, such as vascular endothelial injury and neovascularization of tumors.[3] There were reported studies on the transplanted EPCs distribution in different disease models. In experimental myocardial ischemia rats, 70% of the transplanted EPCs were localized in the spleen and liver at 1–4 days after tail vein injection.[4] In 2018, Higuchi et al.[5] reported the survival of transplanted endothelial progenitor cells in the rat heart. From their PET images we could see transplanted EPC mainly distributed in the liver and neck neoplasms at 1 or 3 day after injection to the left ventricle. The immunofluorescence assays in lung injury and PAH rat model showed the distribution of transplanted EPCs in lung tissue.[6,7] There are many studies on the mechanism of adhesion between endothelial cells and leukocytes. And it is known that central adhesion molecules on the surface of endothelial cells mediate the contact between endothelial cells and leukocytes. The related adhesion molecules expressed on the vascular endothelium mainly include intercellular cell adhesion molecule 1 (ICAM-1, CD54), E-selectin (CD62E), P-selectin (CD62P), and vascular cell adhesion molecule 1 (VCAM-1, CD106).[8–11] The adhesion of leukocytes on the vascular endothelial cells mainly involved the engagements of ICAM-1 and VCAM-1 on the endothelial cells with the leukocyte integrin counter-receptors aLb2 (lymphocyte function-associated antigen 1 [LFA-1]), aMb2 (macrophage-1 antigen [MAC-1]) integrin, and a4b1 integrin (very late antigen 4 [VLA-4]) on the leukocyte. These engagements could lead to the activation of (1) Src, RhoA, and Rac-1 and increased cytosolic free calcium ion concentration ($[Ca^{+2}]_i$) in endothelial cells and (2) downstream proteins such as myosin light chain kinase, VE-cadherin, which likely regulates endothelial cell permeability, develops cell tension development, tugs on actin filaments, and loosens the junctions to mediate the adhesion and transmigration of leukocytes and endothelial cells.[12] Numerous studies showed the increased expression

Received 16 March 2020; accepted 27 April 2020;
https://doi.org/10.1016/j.omtm.2020.04.021.

[4]These authors contributed equally to this work.

Correspondence: Li Huo, Department of Nuclear Medicine, Peking Union Medical College Hospital, Chinese Academy of Medical Sciences and Peking Union Medical College (CAMS & PUMC), Beijing 100730, China.
E-mail: huoli@pumch.cn
Correspondence: Jun Yang, Department of Physiology, and Department of Cardiology of the Second Affiliated Hospital, Zhejiang University School of Medicine, Hangzhou 310058, Zhejiang, China
E-mail: yangjunimb@hotmail.com

of adhesion molecules on pulmonary vascular endothelial cells in PAH patients and PAH animal model.[2,12,13] Additional research indicated that the interaction of ICAM1 and β2-integrins mediated the EPCs adhesion in a murine model of myocardial infarction.[14,15] Thus, we investigate the adhesion molecules in our study for further understanding the role of transplanted EPCs in PAH. There are two main subpopulations of human peripheral blood mononuclear cell (hPBMNC)-derived EPCs, early EPCs and late-outgrowth EPCs (L-EPCs), which are characterized by different markers. Early EPCs are monocytes with limited proliferative ability. They release growth factors or cytokines to promote angiogenesis but cannot directly participate in angiogenesis.[16] In contrast, L-EPCs are of nonhematopoietic origin and have the same morphology and functional competency as endothelial cells. They display high proliferative capacity and were reported to incorporate into growing vessels.[17] In this study, we generated EPCs from hPBMCs and confirmed the expression of CD31, CD34, CD144, von Willebrand factor (vWF), CD146, and vascular endothelial growth factor receptor 2 (VEGFR2, KDR), without CD45 and CD14. In addition, these EPCs exhibited strong tube formation *in vitro*. Based on these properties, these EPCs can be classified as L-EPCs.

Different studies have not reached a consensus on changes of the number of EPCs in the peripheral blood of PAH patients.[18–23] Based on this question, Hansmann et al.[24] developed an EPC capture chip to measure the EPC number. Their results showed that the number of EPCs in the peripheral blood was obviously decreased in idiopathic/heritable PAH patients. It was also reported that the decrease in EPCs in the peripheral blood was correlated with worse hemodynamic clinical parameters in idiopathic PAH (iPAH) patients.[20] Previous studies indicate that transplantation of EPCs has beneficial effects in monocrotaline (MCT)-induced PAH models, suggesting the promising clinical application of EPC therapy.[25,26]

However, there is a lack of *in vivo* imaging evidence of exogenous EPCs accumulating at intimal lesions of the pulmonary artery in PAH and related animal models. Real-time imaging to monitor the dynamics of EPC trafficking in both animals and patients may reveal the mechanism of effective treatment.[27] Therefore, tracing exogenous EPCs *in vivo* and evaluating the safety of EPC transplantation are important for the application of cell therapy.

Various molecular imaging techniques, including fluorescence, bioluminescence, metabolic labeling, single photon emission computed tomography (SPECT), and magnetic resonance imaging (MRI), have been developed and used for EPC labeling and tracking. Radionuclide imaging provides higher sensitivity and is easier to be quantified than other methods.[28] PET offers great advantages over SPECT because of its higher resolution and sensitivity. A previous study showed that the ^{124}I PET allowed successful visualization of EPCs.[29] However, it is an indirect technique with some limitations. Zirconium-89, a commercially available cyclotron-produced PET radionuclide, is promising for application in cell trafficking due to its optimal half-life ($t_{1/2}$ = 78.4 h) and high spatial resolution.[30] ^{89}Zr PET is also suitable for clinical practice, and some ^{89}Zr radiolabeled clinical trials are in process.[31]

In this study, to better understand the role of EPCs in PAH, we applied the ^{89}Zr-oxine cell tracking method and employed micro-PET/CT imaging to monitor the distribution of labeled EPCs in healthy and MCT-induced PAH rats. To confirm the results of PET-CT, we first applied CellVizio confocal microscopy to observe the transplanted EPCs in pulmonary vasculature.

RESULTS

Generation and Phenotypic Identification of EPCs from hPBMNCs

We isolated hPBMCs from healthy volunteers. After incubation for 24 h, most hPBMCs settled to the coated surface at the bottom of the flask (Figure 1A, upper left). After removing the non-adherent cells, the remaining attached cells were cultured with colonies formed after about 2 weeks (Figure 1A, upper right). The subcultured colonies were maintained in endothelial culture medium with the appearance of typical endothelial morphology (Figure 1A, lower left). These selected EPCs exhibited a strong ability to form tube networks *in vitro* (Figure 1A, lower right). Then, we identified these EPCs as L-EPCs with endothelial cell-specific markers by immunofluorescence staining and flow cytometry. They expressed endothelial-representative markers, including CD31 (positive cell percentage, mean ± SD, 97.70% ± 1.87%, n = 3), CD144 (94.50% ± 2.72%, n = 3), vWF (68.87% ± 3.66%, n = 3), CD146 (74.88% ± 5.17%, n = 3), and KDR (69.90% ± 2.51%, n = 3). Moreover, they had moderate CD34 expression (positive cell percentage, 44.27% ± 1.95%, n = 3) and were proved as progenitor cells without hematopoietic properties, demonstrated by the absence of CD45 (positive cell percentage, 0.60% ± 0.26%, n = 3) and CD14 (0.93% ± 0.30%, n = 3; Figures 1B and 1C).

Quality Control of Radiolabeling Product and the Viability and Proliferation of ^{89}Zr-oxine-EPCs

Schematic diagram of ^{89}Zr-oxine labeling EPCs is showed in Figure 2A. ^{89}Zr-oxine complex has planar construction and supports the concept that neutral and lipid-soluble oxine conjugates permeabilize the cell membrane. After ^{89}Zr-oxine complex enters the cytoplasm, ^{89}Zr becomes attached to cytoplasmic components (such as lactoferrin). EPCs were incubated with the ^{89}Zr-oxine complex in PBS at 37°C for 30 min. The percentage of the radiolabeled EPCs was 27.10% ± 11.04% (n = 3) in this radiolabeling procedure. As shown in Figures 2B and 2C, the radiochemical purity of ^{89}Zr-EPCs was 100% after purification of the radiolabeling product. Furthermore, we found that the radiochemical purity by radio-instant Thin Layer Chromatography (iTLC) of stored ^{89}Zr-EPCs was also 100% at 13 h after product purification (Figure 2D). Cell viability of the radiolabeled EPCs was greater than 80% at both time points (0 h, 85.59% ± 3.07%, n = 3; 16 h, 84.07% ± 2.01%, n = 3). The results of the proliferation assay of unlabeled EPCs and ^{89}Zr-EPCs are shown in Figure 2E. EPCs with and without ^{89}Zr-oxine labeling underwent similar proliferation trends within 72 h. There was a linear relationship of cell number with time within 72 h, and a plateau stage was reached at 72–96 h. However, the proliferation rate of ^{89}Zr-EPCs was lower than that of the unlabeled EPCs at the later time points

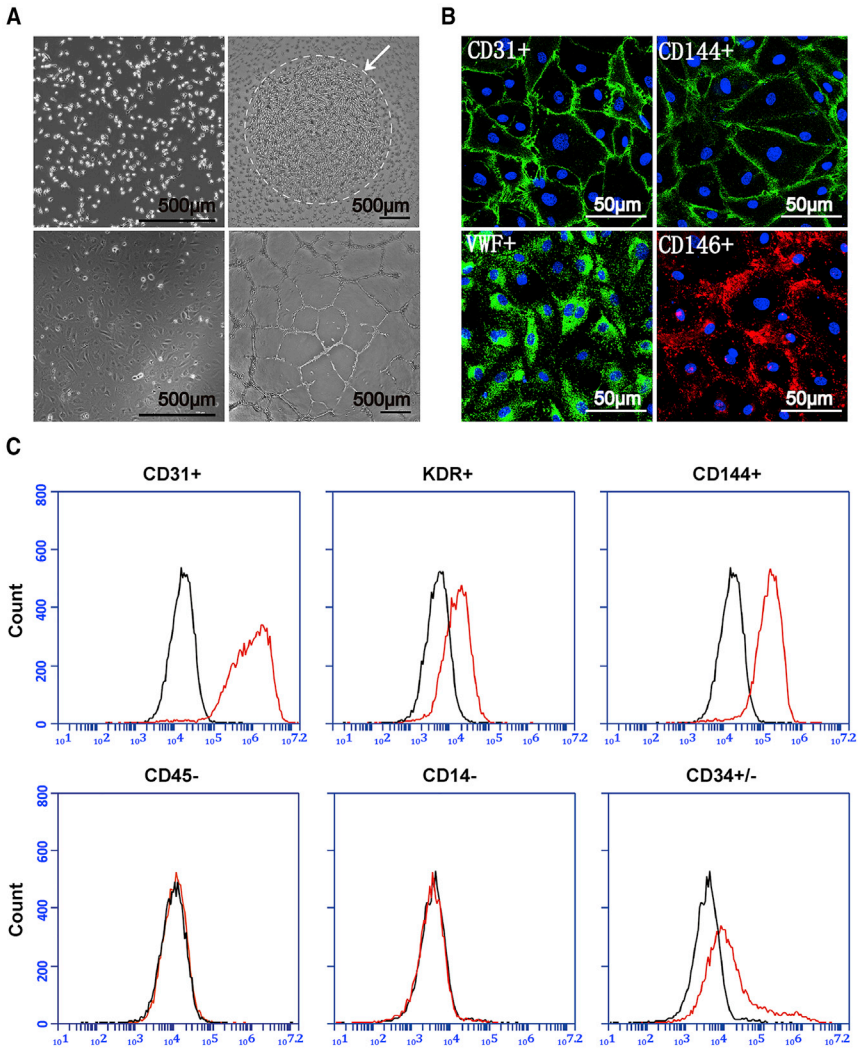

Figure 1. Generation and Phenotypic Identification of EPCs from Human Peripheral Blood Mononuclear Cells

(A) Morphology of (upper left) mononuclear cells 24 h after inoculation. EPCs colonies formed (upper right) after 10–14 days culture. After passaging, the predominant cell type exhibits a cobble stone morphology (lower left) and is able to form endothelial cell-like networks *in vitro* (lower right). Scale bar, 500 μm. (B) Immunostaining assay of EPCs *in vitro*, CD31 (green; DAPI, blue), CD144 (green; DAPI, blue), vWF (green; DAPI, blue), and CD146 (red; DAPI, blue); Scale bar, 50 μm. (C) Flow cytometric analysis of L-EPCs *in vitro*. The red lines represent the L-EPCs labeled with different antibodies. The black lines denote the negative control.

(48 h, $p = 0.0003$; 72 h, $p < 0.0001$; 96 h, $p < 0.0001$; $n = 5$ for each time point). Taken together, our results indicate that ^{89}Zr-oxine labeling of EPCs is efficient and stable.

PET Imaging of ^{89}Zr-oxine-Labeled EPCs in Healthy Rats following Intravenous Injection

Representative images of microPET/CT scans are shown in Figure 3A, and statistical plots of the percentage of injected radioactive dose per gram (%ID/g)-mean values of radioactive substances in animal organs and tissues at each time point are shown in Figure 3B ($n = 4$ rats for each time point). After intravenous injection, EPCs were mainly distributed in the liver, spleen, lung, and joints, followed by the heart, kidney, stomach, and bone (tibia), and the distribution in other tissues (intestine, bladder, brain, and muscle) was low. Radioactivity uptake in the lung reached its peak value at 1 h after administration, while the liver and spleen reached their peak value at 72 h after administration. The representative graphs with the delineated regions of interest (ROIs) of organs marked are shown in Figure S1, and the reconstructed spatial graphs (short videos) are also provided in Video S1. The CellVizio confocal images also showed the distribution of EPCs in liver and spleen 72 h after administration (data not shown). Moreover, radioactive value determination of rat organs *ex vivo* by γ-counting also showed similar distribution characteristics of EPCs after intravenous administration (see Table S1, $n = 5$ rats for each time point).

The Distribution of EPCs in the Pulmonary Vasculature of Healthy and MCT-PAH Rats

After 21 days of MCT administration, right ventricular systolic pressure (RVSP) and the ratio of right ventricular weight to left ventricular plus septal weight (RV/[LV+S]) were measured and significantly elevated as compared with those in the control group (Figure 4A). Moreover, representative H&E staining results showed the obstruction of small blood vessels with thickened medial walls in MCT rats (Figure 4B). The upper graph is from control rat, and the lower one is from MCT rat. Representative confocal images of the lung sections from healthy and MCT-induced PAH rats (1 h after EPCs injection) are shown in Figure 4C, from which we could see the distribution of EPCs in pulmonary blood vessel. The pulmonary blood vessel smooth muscle cells were detected by immunofluorescence staining with anti-rat SM22α, as shown in red. EPCs were detected by immunofluorescence staining with anti-human CD31, which is a specific primary antibody for human CD31 without overlapping selectivity for rat, as shown in green. EPCs were accumulated more in the lungs of PAH than the control rats (Figure 4D: EPCs number in each section: control, 0.43 ± 0.32; MCT-PAH, 1.22 ± 0.41; $p < 0.01$; $n = 6$ rats for each group). Before lung tissue collection, heart perfusion and lung tissue perfusion were carried out, so the EPCs flowing in the blood were almost washed out. The number of EPCs observed in lung section was small, with an average of less than 2 cells in each field, which could be considered to be attached

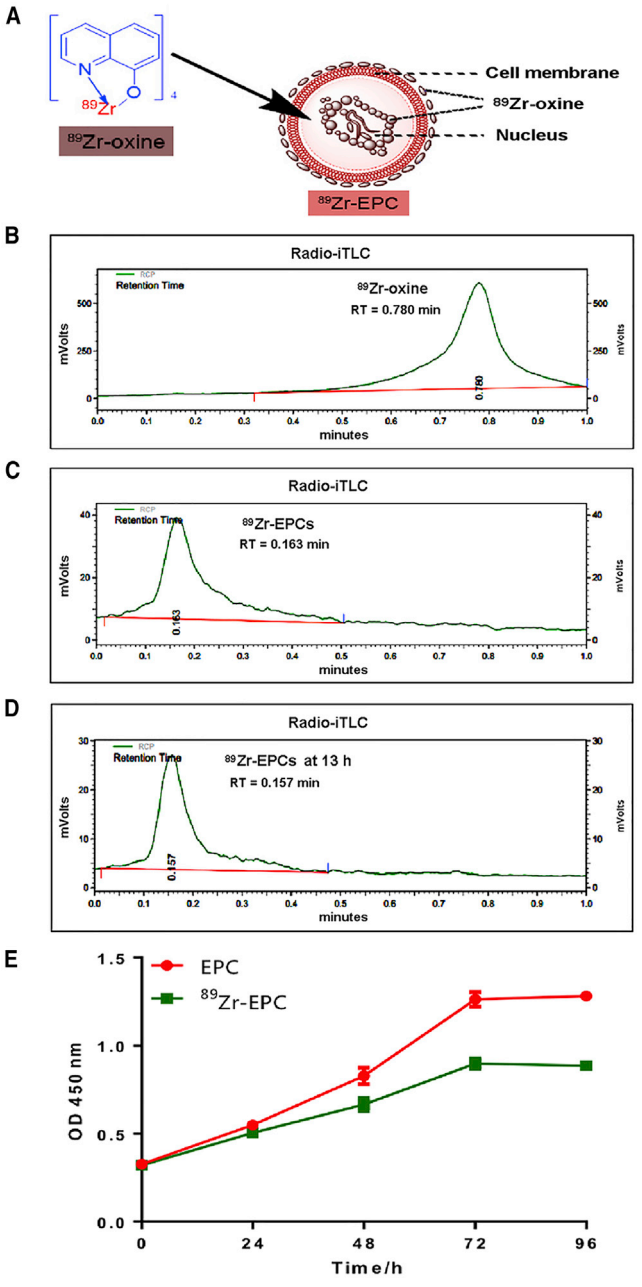

Figure 2. Quality Control of ^{89}Zr-oxine-EPCs and Proliferation Assay

(A) Schematic diagram of ^{89}Zr-oxine labeling EPC cell. ^{89}Zr could enter the cytoplasm and attach to cytoplasmic components. (B) Radio-iTLC of free ^{89}Zr-oxine; iTLC, instant thin-layer chromatography. (C) Radiochemical purity of ^{89}Zr-oxine-EPCs was 100% by radio-iTLC. (D) *In vitro* stability of ^{89}Zr-oxine-EPCs, which were preserved in EPCs complete medium for 13 h. Radiochemical purity of ^{89}Zr-oxine-EPCs at 13 h was 100% by radio-iTLC. (E) Proliferation assay of unlabeled EPCs and ^{89}Zr-oxine-EPCs (data are represented as mean ± SD, n = 5 per time point).

cells. From the CellVizio confocal images (Figure 4E), we could see the abnormal vascular morphology of the MCT-PAH rat lung, and the DiO-labeled EPCs binding in the pulmonary microvasculature of each group (see Videos S2 and S3). The red fluorescence showed that the vascular morphology of MCT-PAH rat lung is of uneven thickness compared with control group, which is consistent with the result of Figure 4B. The green fluorescence indicated that the labeled EPCs stay in the pulmonary vascular and do not move with blood flow (Videos S2 and S3), which could also corroborate the result of Figure 4C. EPCs were accumulated more in the MCT-PAH than the control group (Figure 4F, EPCs number in each section; control, 2.2 ± 0.82; MCT-PAH, 6.40 ± 1.20; $p < 0.01$; n = 3 rats for each group).

Whole-Body MicroPET/CT Imaging Exhibits Increased ^{89}Zr-oxine-EPCs Accumulation in MCT-PAH Rats

To further evaluate ^{89}Zr-oxine labeling as a quantitative tool for tracing EPCs *in vivo*, we intravenously delivered 2×10^6 EPCs into the tail vein of MCT-induced PAH rats. ^{89}Zr-oxine-labeled EPCs were injected intravenously into healthy and PAH rats, and images were recorded over 10 days (n = 4 rats for each time point) (Figure 5). Similar to the distribution in healthy rats, the highest radioactivity was found in the lungs of PAH rats in the first h. Then, most of the radioactivity was found in the liver, spleen, and joints in the next 10 days. As shown in Figure 6A, we also found that the radioactive uptake at different segments in the lungs was higher in PAH than in the control rats 24 h after injection. Furthermore, our statistical data (Figure 6B) confirmed that radioactivity uptake in the lungs of PAH rats was significantly higher than the control group at 24, 72, 168, and 254 h post-injection (n = 3 rats for each time point). In general, these data demonstrated the enrichment of EPCs in the affected pulmonary vasculature of PAH rats.

The Increased Accumulation of EPCs in PAH Lungs Was Mediated by Chemokine and Cell Adhesion Molecules

The experimental procedures of transwell and attachment assays are shown in Figure 7A, and the detailed methods were provided in the Supplemental Information. The transwell migration assay results showed that plasma from both MCT-PAH rats and iPAH patients could increase the migration of EPCs (Figures 7B and 7C; EPCs counts: control rat plasma, 265.4 ± 89.6; MCT-model, 522.5 ± 99.1; healthy volunteer, 143.6 ± 38.7; iPAH patient, 232.1 ± 44.2, $p < 0.01$ for both comparisons). Human pulmonary arterial endothelial cells (HPAECs) were treated with plasma from healthy volunteers or iPAH patients, and we found that the number of EPCs attached to HPAECs was increased in the plasma of iPAH patients. The increased adhesion of EPCs could be reversed by A205804, a commonly used specific inhibitor of E-selectin and ICAM-1, in the attachment assay (Figures 7D and 7E; attached EPCs counts: control, 19.2 ± 7.6; control+-inhibitor, 12.1 ± 4.6; iPAH, 37.1 ± 4.8; iPAH+inhibitor, 11.3 ± 5.5; $p = 0.014$ for iPAH versus control, and $p = 0.002$ for iPAH+inhibitor versus iPAH). These results indicate that plasma under PAH pathological conditions could upregulate the migration of EPCs and the attachment of EPCs to HPAECs, which could be a possible mechanism of the increased EPCs accumulation in MCT-PAH rats.

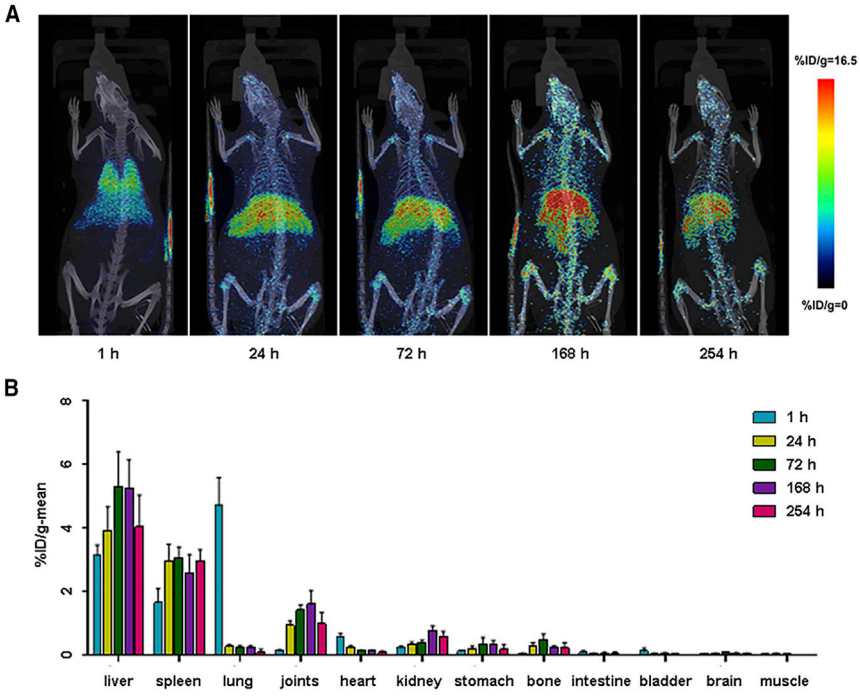

Figure 3. Whole-Body MicroPET/CT Imaging of ^{89}Zr-oxine-EPCs in Healthy Rats

(A) Maximum intensity projections (MIPs) of representative rats are shown at several time points after injection. ^{89}Zr-oxine-EPCs were distributed primarily in the lung at 1 h and then migrated mainly to the liver and spleen. (B) Statistical plots of the radioactive values (%ID/g-mean) of organs and tissues of rats at five time points post-injection. Plot bar, mean ± SD; n = 4 rats for each time point.

DISCUSSION

A noninvasive and high-quality imaging technique is required to understand the pathogenesis of the disease and provide visual evidence for cell therapy. To the best of our knowledge, there is no report on high-quality PET imaging of EPCs by direct radiolabeling. Oxine is a safe chelating agent commonly used for clinical monitoring leukocyte metabolism.[32] Among various PET nuclides, ^{89}Zr is the most ideal choice with a long physical half-life and high γ-energy.[33] ^{89}Zr-oxine PET has been proven to be an effective method for cell trafficking in some disease models.[34] With ^{89}Zr-oxine PET, we showed the relocation of EPCs from the lungs to the liver and spleen dynamically, consistent with previous reports showing the bone marrow cell distribution.[32]

In this study, we visualized the distribution of transplanted EPCs in normal rats and PAH rats. Intravenously administered ^{89}Zr-labeled EPCs were distributed primarily to the lung at 1 h. And the quantitative results showed that the number of EPCs recruited to the lungs were significantly higher in MCT-induced PAH rats after 24 h of injection, which indicated that L-EPCs were more likely attached to the injured blood vessels of MCT-induced PAH rats than the healthy blood vessels. In addition, our study by immunofluorescence staining on the lung slices and CellVizio confocal of superficial layer in the lung of rats had revealed that the transplanted EPCs could attach to the pulmonary vasculature of both healthy and MCT-PAH rats, and there are more EPCs binding to the pulmonary vasculature intimal lesion site of PAH rats, which would help us clarify the role of EPCs in vascular remodeling and repairment and also confirmed the results we obtained from the PET imaging. Together, both the overall distribution and microscopic localization of the transplanted EPCs could demonstrate the possibility of transplanted EPCs repairing the pulmonary vasculature. Moreover, we could see the transplanted EPCs subsequently migrated to the liver and spleen at 24 h after administration. Previous research also reported that EPCs mainly distribute in rat liver, spleen, and neck neoplasms 1 day after injection.[4,5] This indicated that some EPCs might be eliminated by the immune system and the main immune organs involved are liver and spleen. Therefore, a long-term observation of the function of the patients' liver and spleen after treatment with EPCs therapy is necessary.

An increasing number of studies have demonstrated that EPCs play an essential role in endothelium repairment in related diseases, including ischemic cardiovascular diseases and PAH.[35,36] EPCs promote the formation and maintain the function of normal blood vessels.[37,38] EPCs from iPAH patient or PAH patients with bone morphogenetic protein type II receptor (*BMPR2*) mutations exhibited impaired vasculogenic activity.[23] It has been suggested that due to the reduced EPCs capability, the PAH patient-derived EPCs recruited to the injury site cannot fully repair the vasculature damage.[39,40] In addition, genetic modification or drug pretreatment might be able to restore the intact function of patient-derived EPCs.[41] Therefore, genetic modification and drug pretreatment could be potential strategies to improve the efficacy of cell therapy.

In our results, we found the presence of EPCs in the pulmonary vasculature and the increased accumulation of EPCs in the lungs of MCT-induced PAH rats. What's the reason of the increased accumulation? We speculate that a self-compensation mechanism was activated in MCT-induced PAH rats and PAH patients. The increased the serum levels of some specific cytokines and adhesion molecules could attract more EPCs to pulmonary vascular lesions; meanwhile, it is also possible that inflammation and increased permeability could result in greater cell persistence in the pulmonary vascular lesions of PAH. Previous studies showed that some specific cytokines and adhesion molecule (interleukin-4 [IL-4], IL-13, P-selectin, and ICAM-1) levels were markedly upregulated in the endothelium of iPAH, as well as MCT-rat pulmonary arteries.[2,12,13] There are also reported

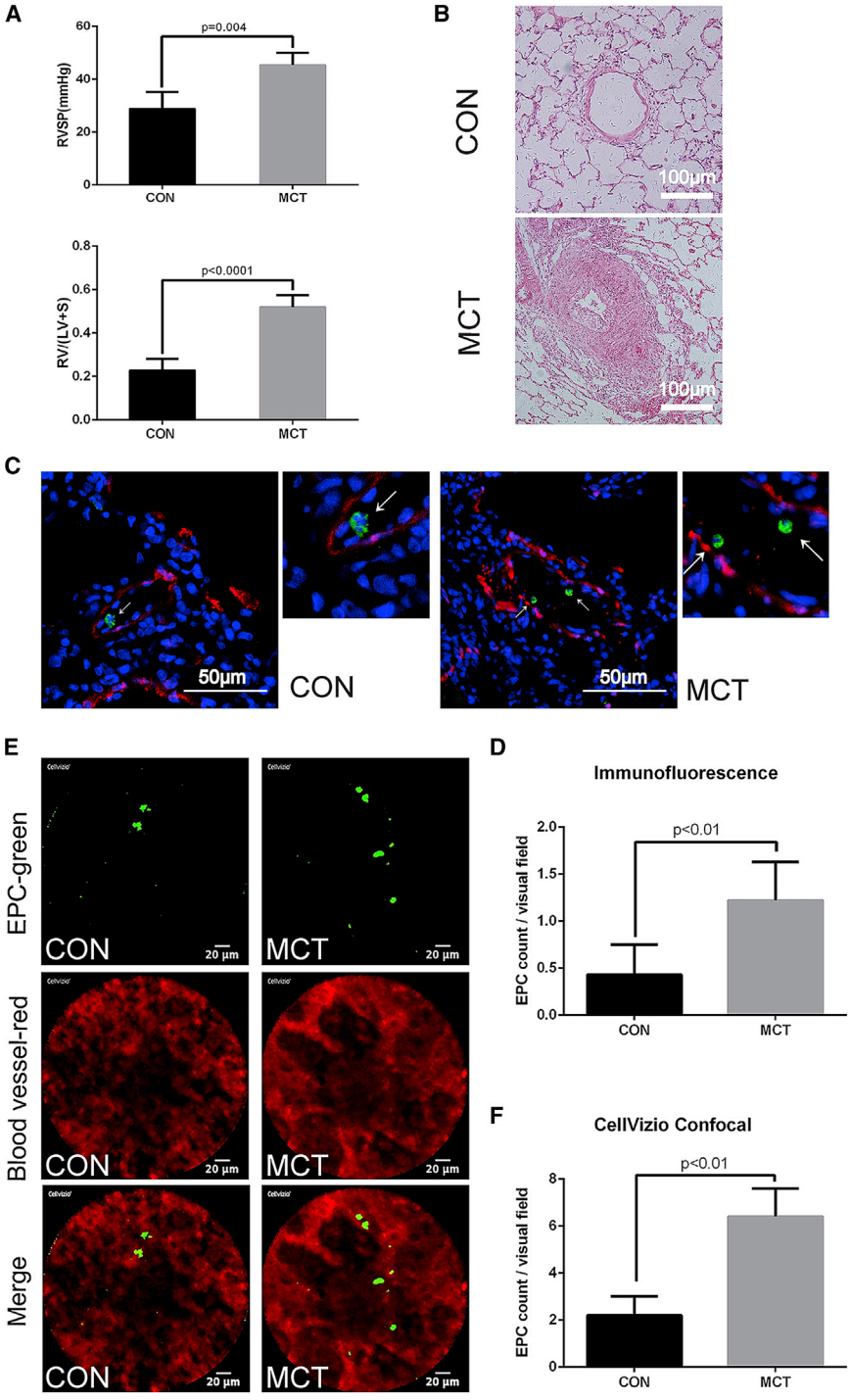

Figure 4. Establishment of MCT-PAH Model and the Distribution of EPCs in the Pulmonary Vasculature of Healthy and PAH Rats

(A) The RVSP and RV/(LV+S) of the control and PAH-model groups (n = 6 in each group). (B) Representative H&E staining from control and PAH rats of blood vessels. Scale bar, 100 μm. (C) Representative confocal images of immunofluorescence staining of slices for CD31 (green) and SM22α (red) from lung sections of rats injected with EPCs. Arrows indicate EPCs. Nuclei were stained with 4′,6-diamidino-2-phenylindole (DAPI) (blue). Scale bar, 50 μm. (D) Statistical plot showing the EPCs number of each section in both groups of (C) (data are represented as mean ± SD, n = 6, three slices were observed for each rat, 5 random visual fields were selected per slice for statistical analysis). (E) Representative confocal images of CellVizio confocal of lung of rats after injected with DiO-labeled EPCs. DiO-labeled cells are green, and blood with Evans blue is red. Scale bar, 20 μm. (F) Statistical plot showing the EPCs number of each section in both groups of (E) (data are represented as mean ± SD, n = 3, nine random visual fields were selected per rat for statistical analysis).

studies supporting the existence of endothelial cells migration-promoting and adherence-increasing cytokines, chemokine and cell adhesion molecules, from the PAH serum, including E-selectin and ICAM-1.[42–44] In our results, plasma under pathological conditions upregulated the migration of EPCs and the attachment of EPCs to HPAECs. A205804 is a commonly used specific inhibitor of E-selectin and ICAM-1,[45] and it suppressed the increased attachment of EPCs induced by PAH plasma. From the results of this and previous studies, it was suggested that the migration of EPCs and the expression of cell adhesion molecules of HPAECs could be upregulated under the pathological condition of PAH. This would be a research direction for further understanding the mechanism of the higher accumulation of transplanted EPCs in the lungs of PAH rats.

In summary, we applied an ^{89}Zr-oxine radiolabeling technique for labeling and tracking EPCs efficiently in a preclinical study. Quantitative PET-CT imaging on ^{89}Zr-oxine EPCs could be optimized for noninvasive monitoring EPCs in clinical practice. Together the PET/CT result, we first applied CellVizio confocal microscopy to observe micro co-localization of transplanted EPCs and fluorescent blood vessels in lung and other organs. Our results revealed that the distribution of EPCs *in vivo* and the higher accumulation of EPCs in the lungs of MCT-induced PAH rats, which would be beneficial for optimizing the efficacy and safety of EPCs transplantation in clinic. In addition, our study indicated that the increased cytokines and adhesion molecules, such as E-selectin and ICAM-1, could be account for the higher accumulation of EPCs in the pulmonary vasculature. Further work is required to better understand the molecular

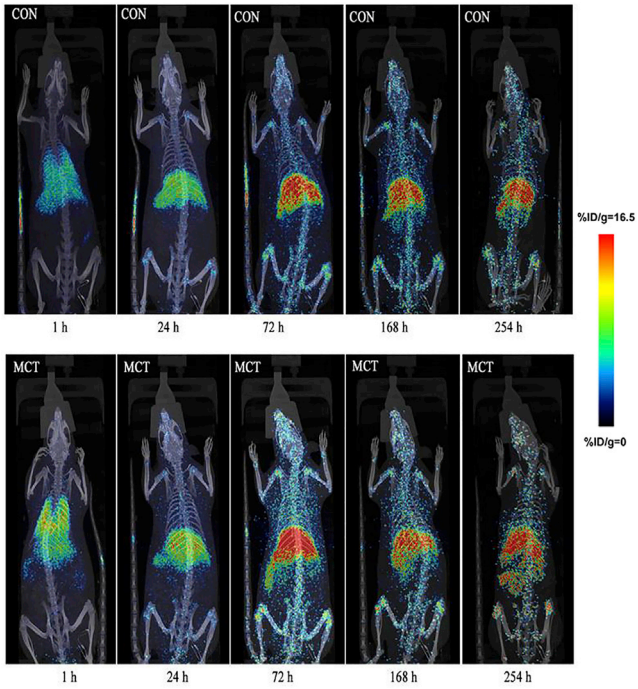

Figure 5. Whole-Body MicroPET/CT Imaging Showing Increased ^{89}Zr-oxine-EPCs Accumulation in PAH Compared with Control Rats

Maximum intensity projections (MIPs) of representative rats are shown at five time points after intravenous injection. ^{89}Zr-oxine-EPCs were distributed primarily to the lung at 1 h and then migrated to the liver and spleen in both control and PAH rats. The accumulation of EPCs in the lungs of PAH rats was higher than that in healthy rats at different time points. The liver and spleen also showed moderate to considerable accumulation in both control and PAH groups (n = 4 rats per time point in each group).

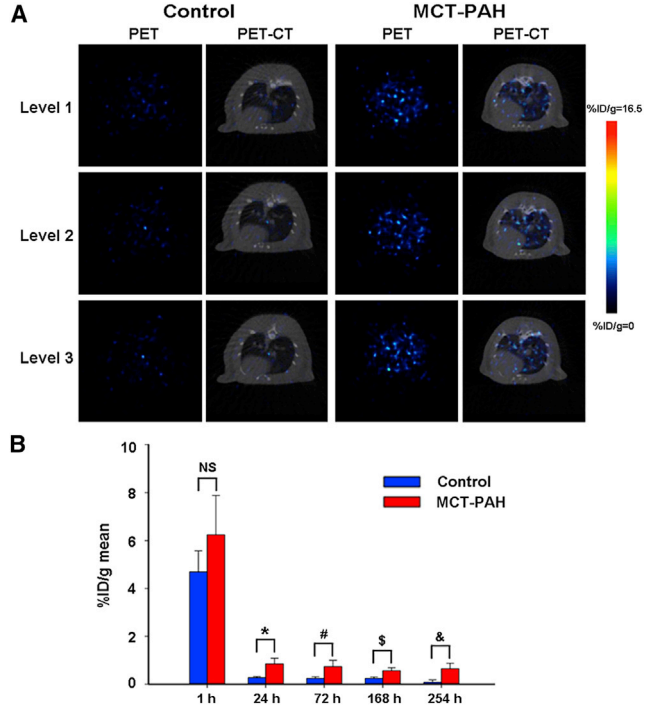

Figure 6. Representative Axial Section Imaging and Quantitative Analysis of ^{89}Zr-oxine-EPCs in Control and PAH Rats

(A) Representative axial section PET imaging and PET/CT images of rats 24 h after cell transplantation of the radiolabeled EPCs. (B) Quantitative analysis of the radioactivity uptake in the lungs of the control and PAH-model groups. %ID/g-mean, radioactive uptake values; NS, no significant difference; $^{*}p = 0.02$, $^{\#}p = 0.02$, $^{\$}p = 0.021$, $^{\&}p = 0.021$; data are represented as mean ± SD, n = 3 per time point for each group.

mechanism of E-selectin and ICAM-1 in the accumulation of transplanted EPCs, as well as to increase the expression of these factors on EPCs by applicable strategy to improve the effect of EPC transplantation.

MATERIALS AND METHODS

Animals

Specific pathogen free male Sprague-Dawley (SD) rats weighing 160–200 g (6 weeks old) were purchased from Beijing Vital River Laboratory Animal Technology. The ethics review committee of Institute of Basic Medical Sciences, Chinese Academy of Medical Sciences approved the animal studies. All experiments were conducted in compliance with the National Research Council guidelines, as well as the relevant laws and institutional guidelines of Beijing Union Hospital.

Preparation and Identification of Human EPCs

Peripheral blood from healthy volunteers was used for the isolation and generation of EPCs. hPBMNCs were isolated by Ficoll (BD Biosciences) density-gradient centrifugation. The detailed methods of EPC culture are provided in the Supplemental Information. All sample collections were performed under the approval of the ethical review board of Institute of Basic Medical Sciences, Chinese Academy of Medical Sciences (IBMS, CAMS, 014-2015). The patients donated blood after providing informed consent. The cells were assessed by immunostaining using CD31, CD144, and vWF, CD146, and flow cytometry using CD31, KDR, CD144, CD34, and CD14, as previously described.[46] For the tube formation assay, a total of 2×10^4 cells were seeded into a 48-well plate precoated with Matrigel. Tube formation was detected at 4 h post seeding.

MCT-Induced PAH Rat Model

The specific method of animal model establishment is provided in the Supplemental Information. 3 weeks after MCT injection, the RVSP of 6 rats from each group was monitored by a BL-420S physiological experiment system, and RV/(LV+S) was calculated to identify right ventricular hypertrophy of the rats. After confirming the success of MCT-PAH model establishment by testing RVSP and RV/(LV+S), the remaining rats of the CON and MCT-PAH groups were ready for EPCs injection.

H&E & Immunofluorescence (IF) Staining

After dewaxing, the rat lung slices were treated with routine H&E staining and IF staining. The methods are provided in the Supplemental Information.

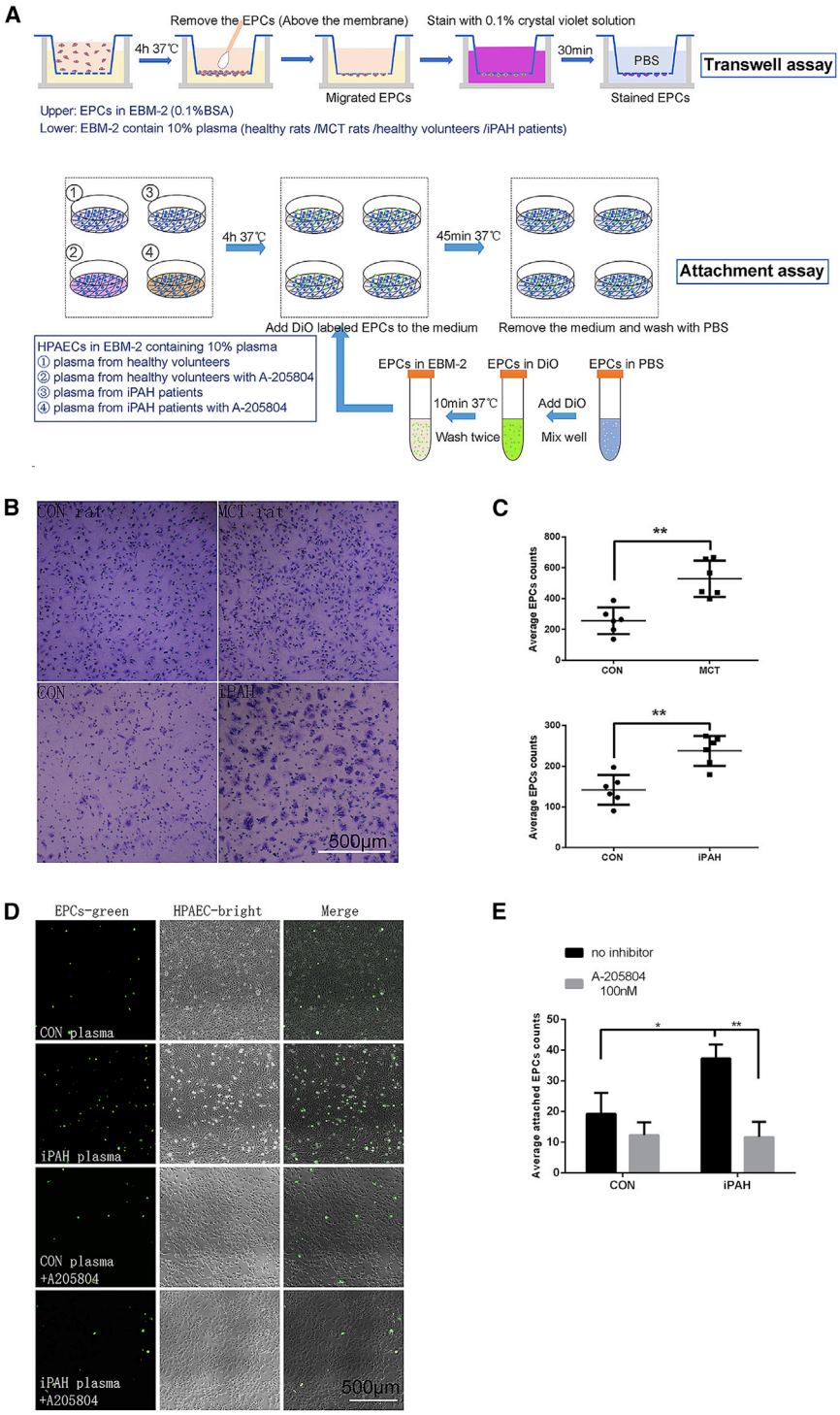

Figure 7. The Increased Accumulation of EPCs in PAH Lung Was Mediated by Chemokine and Cell Adhesion Molecules

(A) Schematic experimental designs of transwell and attachment assays. (B) Representative light images of the transwell migration assay of EPCs induced by plasma from healthy rats, MCT-PAH rats, healthy volunteers, and iPAH patients. Cells on the lower surface were stained with crystal violet. Scale bar, 500 μm. (C) Statistical results of staining and cell counting after the transwell migration assay. Data are represented as mean ± SD, $p < 0.01$ for both comparisons. Cells were counted after staining with crystal violet, and n = 6 in each group. (D) Representative images of the attachment assay of EPCs and HPAECs treated with basic medium containing different plasma (from healthy volunteers or iPAH patients) with or without 100 nM A-205804. EPCs were labeled with DiO (green). Scale bar, 500 μm. (E) Statistical plot showing the attached EPCs number of each section in both groups of (D). Data are represented as mean ± SD, $p = 0.014$ for iPAH versus control, and $p = 0.002$ for iPAH+inhibitor versus iPAH. Fluorescent cells in 5 fields were counted for each condition. n = 4 for each group.

^{89}Zr-oxine Labeling of EPCs

^{89}Zr was produced at Perkin Elmer Healthy Sciences (the Netherlands). The ^{89}Zr-oxine complex was synthesized from ^{89}Zr-oxalate and oxine following a previously reported method.[47] First, we neutralized the ^{89}Zr-oxalic acid with 1 M Na_2CO_3 and adjusted the solution pH value to 7. We added the oxine dissolved in chloroform to the above solution and adequately mixed the solution for 15 min on the vortex mixer to make sure there was a full reaction. Then the mixed solution with reaction product was separated into two phases by centrifugation. After removing the water phase, chloroform was evaporated at 60°C, and then the sediment was redissolved by adding a little amount of DMSO (100 μL) and an equal volume of cell medium (in order to conveniently control the final DMSO content in the cell medium in radiolabeling process below 5%). Radiolabeling of EPCs with ^{89}Zr-oxine was accomplished using the previously described method.[32] An amount of 5∼6 × 10^6 EPCs in cell medium was added with 100∼200 μCi of ^{89}Zr-oxine and hatched at 25°C for 20∼30 min. The reacted solution was centrifuged with PBS to remove the free ^{89}Zr-oxine. The cell precipitation was resuspended and the final labeling product ^{89}Zr-EPC cells were prepared. Radiolabeled cells were washed twice with cell medium prior to the subsequent experiments.

Assessment of Cell Viability and Proliferation

The methods of assessment of cell viability and proliferation are provided in the Supplemental Information.

EPCs Tracking by MicroPET/CT

Whole-body imaging was performed using a micro-PET/CT (Pingseng HealthCare, Suzhou, China). Rats were anesthetized with

isoflurane/O_2. After intravenous injection of ^{89}Zr-oxine-EPC (2×10^6 cells at 185 kBq/10^6 cells), static whole-body PET/CT scans were performed at 1 h, 24 h, 72 h, 168 h, and 254 h after administration with an acquisition time of 10 min per imaging point. After reconstructing the scanned raw data, the image and data analyses were carried out using the PMOD software by a statistical investigator who was blind to the experimental design and grouping. The heart, liver, spleen, lung, muscle, tibia, and other organs were delineated as ROIs. The ROIs were delineated by manual selection of the statistical investigator blind to experimental design in the reconstructed spatial images according to a previously reported method.[48] After delineation, the radioactivity values of the ROIs per unit volume were obtained, and the percentage injected dose per gram (%ID/g) values of each organ were calculated. In order to scan and quantify the amount of radiation in various organs of the whole body at different time points, and it took 10 min for each time point to scan the whole body layer by layer, so static whole body layer-by-layer scanning and acquisition was used in this study.

DiO-Labeled EPCs Detected by CellVizio Confocal

(1) DiO labeling of EPCs was as follows: 2×10^6/mL EPCs suspension (EBM-2 without serum) were made after trypsin digestion. DiO (Invitrogen, USA, V-22886) was added to the cell suspension according to the instruction. After incubation at 37°C for 10 min, the cells were washed twice with DPBS before injecting into the rat tail vein. (2) Fluorescence labeling of blood vessel was as follows: 1 h after injection, rats were anesthetized with isoflurane/O_2. 1.2% Evans blue (Abcam, UK, ab120869) was intravenously injected to rats (1 mL for each rat). (3) CellVizio confocal was as follows: labeled EPCs and blood vessels were detected by CellVizio Dual Band confocal endoscopy system *in vivo*. We opened the chest and exposed the rat lung and used the Mini-Z microprobe to scan the rat lung (the probe touches the lung directly). The working distance of Mini-Z microprobe is 70 μm. Labeled EPCs could be observed at 488 nm and the blood vessel could be observed at the wavelength of 660 nm.

EPCs Migration and Attachment on Stimulated HPAECs

The detailed incubation conditions and procedures of migration and attachment assays are shown in the Supplemental Information.

Data Analysis

Results were presented as means ± SD. Data of each group were treated with the normal distribution test (Shapiro-Wilk test). Statistical significance between two groups was determined using Student's t test (for normal distribution) or Mann-Whitney U test (for non-normal distribution). p values below 0.05 were considered statistically significant.

SUPPLEMENTAL INFORMATION

Supplemental Information can be found online at https://doi.org/10.1016/j.omtm.2020.04.021.

AUTHOR CONTRIBUTIONS

J.Y. and L.H. participated in study design, revised the manuscript, and agreed to be accountable for all aspects of the work. J.Y. finalized submission. Y.L. and X.Z. participated in the design of the study, data acquisition, statistical analysis, and drafting of the manuscript. J.D., Y.X., M.Z., and X.W. participated in cell culture, radiolabeling, and animal experiments. W.Z. participated in the imaging data analysis. All authors provided final approval of the version to be published.

CONFLICTS OF INTEREST

The authors declare no competing interests.

ACKNOWLEDGMENTS

We would like to thank MITRO Biotech for providing technical support on microPET/CT and Lihong Sun from the Center for Experimental Animal Research (Institute of Basic Medical Sciences, Chinese Academy of Medical Sciences) for providing technical support on CellVizio confocal. And we also thank L.H. and J.Y. for donating their blood samples to generate EPCs. This work was sponsored in part by the National Key Research and Development Program of China Stem Cell and Translational Research (grant number 2016YFA0102300); the National Natural Science Foundation of China (grant number 81571713); CAMS Innovation Fund for Medical Sciences (grant number CIFMS 2016-I2M-4-003); and CAMS Initiative for Innovative Medicine (grant number CAMS 2018-I2M-3-001). J.Y., ORCID: 0000-0001-9715-8100.

REFERENCES

1. Keighron, C., Lyons, C.J., Creane, M., O'Brien, T., and Liew, A. (2018). Recent Advances in Endothelial Progenitor Cells Toward Their Use in Clinical Translation. Front. Med. (Lausanne) *5*, 354.
2. Le Hiress, M., Tu, L., Ricard, N., Phan, C., Thuillet, R., Fadel, E., Dorfmüller, P., Montani, D., de Man, F., Humbert, M., et al. (2015). Proinflammatory Signature of the Dysfunctional Endothelium in Pulmonary Hypertension. Role of the Macrophage Migration Inhibitory Factor/CD74 Complex. Am. J. Respir. Crit. Care Med. *192*, 983–997.
3. Pelosi, E., Castelli, G., and Testa, U. (2014). Endothelial progenitors. Blood Cells Mol. Dis. *52*, 186–194.
4. Aicher, A., Brenner, W., Zuhayra, M., Badorff, C., Massoudi, S., Assmus, B., Eckey, T., Henze, E., Zeiher, A.M., and Dimmeler, S. (2003). Assessment of the tissue distribution of transplanted human endothelial progenitor cells by radioactive labeling. Circulation *107*, 2134–2139.
5. Higuchi, T., Anton, M., Saraste, A., Dumler, K., Pelisek, J., Nekolla, S.G., Bengel, F.M., and Schwaiger, M. (2009). Reporter gene PET for monitoring survival of transplanted endothelial progenitor cells in the rat heart after pretreatment with VEGF and atorvastatin. J. Nucl. Med *50*, 1881–1886.
6. Ju, Y.N., Geng, Y.J., Wang, X.T., Gong, J., Zhu, J., and Gao, W. (2019). Endothelial Progenitor Cells Attenuate Ventilator-Induced Lung Injury with Large-Volume Ventilation. Cell Transplant. *28*, 1674–1685.
7. Yip, H.K., Chang, L.T., Sun, C.K., Sheu, J.J., Chiang, C.H., Youssef, A.A., Lee, F.Y., Wu, C.J., and Fu, M. (2008). Autologous transplantation of bone marrow-derived endothelial progenitor cells attenuates monocrotaline-induced pulmonary arterial hypertension in rats. Crit. Care Med. *36*, 873–880.
8. Li, X., Abdi, K., Rawn, J., Mackay, C.R., and Mentzer, S.J. (1996). LFA-1 and L-selectin regulation of recirculating lymphocyte tethering and rolling on lung microvascular endothelium. Am. J. Respir. Cell Mol. Biol. *14*, 398–406.
9. Schmidt, E.P., Kuebler, W.M., Lee, W.L., and Downey, G.P. (2016). Adhesion Molecules: Master Controllers of the Circulatory System. Compr. Physiol. *6*, 945–973.

10. Sriramarao, P., Anderson, W., Wolitzky, B.A., and Broide, D.H. (1996). Mouse bone marrow-derived mast cells roll on P-selectin under conditions of flow in vivo. Lab. Invest. *74*, 634–643.

11. Steegmaier, M., Blanks, J.E., Borges, E., and Vestweber, D. (1997). P-selectin glycoprotein ligand-1 mediates rolling of mouse bone marrow-derived mast cells on P-selectin but not efficiently on E-selectin. Eur. J. Immunol. *27*, 1339–1345.

12. Kuebler, W.M., Bonnet, S., and Tabuchi, A. (2018). Inflammation and autoimmunity in pulmonary hypertension: is there a role for endothelial adhesion molecules? (2017 Grover Conference Series). Pulm. Circ. *8*, 2045893218757596.

13. Grunig, G., and Durmus, N. (2015). Spotlight on Inflammation in Pulmonary Hypertension. Am. J. Respir. Crit. Care Med. *192*, 913–915.

14. Chavakis, E., Aicher, A., Heeschen, C., Sasaki, K., Kaiser, R., El Makhfi, N., Urbich, C., Peters, T., Scharffetter-Kochanek, K., Zeiher, A.M., et al. (2005). Role of β2-integrins for homing and neovascularization capacity of endothelial progenitor cells. J. Exp. Med. *201*, 63–72.

15. Fujiyama, S., Amano, K., Uehira, K., Yoshida, M., Nishiwaki, Y., Nozawa, Y., Jin, D., Takai, S., Miyazaki, M., Egashira, K., et al. (2003). Bone marrow monocyte lineage cells adhere on injured endothelium in a monocyte chemoattractant protein-1-dependent manner and accelerate reendothelialization as endothelial progenitor cells. Circ. Res. *93*, 980–989.

16. Hu, L., Dai, S.C., Luan, X., Chen, J., and Cannavicci, A. (2018). Dysfunction and Therapeutic Potential of Endothelial Progenitor Cells in Diabetes Mellitus. J. Clin. Med. Res. *10*, 752–757.

17. Yoder, M.C. (2011). Progenitor cells in the pulmonary circulation. Proc. Am. Thorac. Soc. *8*, 466–470.

18. Asosingh, K., Erzurum, S.C., Yoder, M.C., and Tuder, R.M. (2009). Letter by asosingh et Al regarding article, "circulating endothelial progenitor cells in patients with eisenmenger syndrome and idiopathic pulmonary arterial hypertension". Circulation *119*, e230.

19. Asosingh, K., Aldred, M.A., Vasanji, A., Drazba, J., Sharp, J., Farver, C., Comhair, S.A., Xu, W., Licina, L., Huang, L., et al. (2008). Circulating angiogenic precursors in idiopathic pulmonary arterial hypertension. Am. J. Pathol. *172*, 615–627.

20. Diller, G.P., van Eijl, S., Okonko, D.O., Howard, L.S., Ali, O., Thum, T., Wort, S.J., Bédard, E., Gibbs, J.S., Bauersachs, J., et al. (2008). Circulating endothelial progenitor cells in patients with Eisenmenger syndrome and idiopathic pulmonary arterial hypertension. Circulation *117*, 3020–3030.

21. Fadini, G.P., Schiavon, M., Rea, F., Avogaro, A., and Agostini, C. (2007). Depletion of endothelial progenitor cells may link pulmonary fibrosis and pulmonary hypertension. Am. J. Respir. Crit. Care Med. *176*, 724–725, author reply 725.

22. Junhui, Z., Xingxiang, W., Guosheng, F., Yunpeng, S., Furong, Z., and Junzhu, C. (2008). Reduced number and activity of circulating endothelial progenitor cells in patients with idiopathic pulmonary arterial hypertension. Respir. Med. *102*, 1073–1079.

23. Toshner, M., Voswinckel, R., Southwood, M., Al-Lamki, R., Howard, L.S., Marchesan, D., Yang, J., Suntharalingam, J., Soon, E., Exley, A., et al. (2009). Evidence of dysfunction of endothelial progenitors in pulmonary arterial hypertension. Am. J. Respir. Crit. Care Med. *180*, 780–787.

24. Hansmann, G., Plouffe, B.D., Hatch, A., von Gise, A., Sallmon, H., Zamanian, R.T., and Murthy, S.K. (2011). Design and validation of an endothelial progenitor cell capture chip and its application in patients with pulmonary arterial hypertension. J. Mol. Med. (Berl.) *89*, 971–983.

25. Takahashi, M., Nakamura, T., Toba, T., Kajiwara, N., Kato, H., and Shimizu, Y. (2004). Transplantation of endothelial progenitor cells into the lung to alleviate pulmonary hypertension in dogs. Tissue Eng. *10*, 771–779.

26. Zhao, Y.D., Courtman, D.W., Deng, Y., Kugathasan, L., Zhang, Q., and Stewart, D.J. (2005). Rescue of monocrotaline-induced pulmonary arterial hypertension using bone marrow-derived endothelial-like progenitor cells: efficacy of combined cell and eNOS gene therapy in established disease. Circ. Res. *96*, 442–450.

27. de la Puente, P., Muz, B., Azab, F., and Azab, A.K. (2013). Cell trafficking of endothelial progenitor cells in tumor progression. Clin. Cancer Res. *19*, 3360–3368.

28. Wang, S., Fang, J., Zhang, T., Wang, B., Chen, J., Li, X., Zhang, S., and Zhang, W. (2011). Magnetic resonance imaging targeting of intracranial glioma xenografts by Resovist-labeled endothelial progenitor cells. J. Neurooncol. *105*, 67–75.

29. Higuchi, T., Anton, M., Dumler, K., Seidl, S., Pelisek, J., Saraste, A., Welling, A., Hofmann, F., Oostendorp, R.A., Gansbacher, B., et al. (2009). Combined reporter gene PET and iron oxide MRI for monitoring survival and localization of transplanted cells in the rat heart. J. Nucl. Med *50*, 1088–1094.

30. Bansal, A., Pandey, M.K., Demirhan, Y.E., Nesbitt, J.J., Crespo-Diaz, R.J., Terzic, A., Behfar, A., and DeGrado, T.R. (2015). Novel (89)Zr cell labeling approach for PET-based cell trafficking studies. EJNMMI Res. *5*, 19.

31. NIH. ClinicalTrials.gov. https://clinicaltrials.gov/.

32. Asiedu, K.O., Koyasu, S., Szajek, L.P., Choyke, P.L., and Sato, N. (2017). Bone Marrow Cell Trafficking Analyzed by 89Zr-oxine Positron Emission Tomography in a Murine Transplantation Model. Clin. Cancer Res *23*, 2759–2768.

33. de la Fuente, A., Kramer, S., Mohr, N., Pektor, S., Klasen, B., Bausbacher, N., Miederer, M., Zentel, R., and Rösch, F. (2019). ^{68}Ga[Ga]-, ^{111}In[In]-oxine: a novel strategy of *in situ* radiolabeling of HPMA-based micelles. Am. J. Nucl. Med. Mol. Imaging *9*, 67–83.

34. Asiedu, K.O., Ferdousi, M., Ton, P.T., Adler, S.S., Choyke, P.L., and Sato, N. (2018). Bone marrow cell homing to sites of acute tibial fracture: ^{89}Zr-oxine cell labeling with positron emission tomographic imaging in a mouse model. EJNMMI Res. *8*, 109.

35. Harper, R.L., Maiolo, S., Ward, R.J., Seyfang, J., Cockshell, M.P., Bonder, C.S., and Reynolds, P.N. (2019). BMPR2-expressing bone marrow-derived endothelial-like progenitor cells alleviate pulmonary arterial hypertension in vivo. Respirology *24*, 1095–1103.

36. Zhang, B.F., Jiang, H., Chen, J., Hu, Q., Yang, S., and Liu, X.P. (2019). Silica-coated magnetic nanoparticles labeled endothelial progenitor cells alleviate ischemic myocardial injury and improve long-term cardiac function with magnetic field guidance in rats with myocardial infarction. J. Cell. Physiol. *234*, 18544–18559.

37. Asahara, T., and Kawamoto, A. (2004). Endothelial progenitor cells for postnatal vasculogenesis. Am. J. Physiol. Cell Physiol. *287*, C572–C579.

38. Balaji, S., King, A., Crombleholme, T.M., and Keswani, S.G. (2013). The role of endothelial progenitor cells in postnatal vasculogenesis: implications for therapeutic neovascularization and wound healing. Adv. Wound Care (New Rochelle) *2*, 283–295.

39. Chen, H., Strappe, P., Chen, S., and Wang, L.-X. (2014). Endothelial progenitor cells and pulmonary arterial hypertension. Heart Lung Circ. *23*, 595–601.

40. Diller, G.-P., Thum, T., Wilkins, M.R., and Wharton, J. (2010). Endothelial progenitor cells in pulmonary arterial hypertension. Trends Cardiovasc. Med. *20*, 22–29.

41. Granton, J., Langleben, D., Kutryk, M.B., Camack, N., Galipeau, J., Courtman, D.W., and Stewart, D.J. (2015). Endothelial NO-Synthase Gene-Enhanced Progenitor Cell Therapy for Pulmonary Arterial Hypertension: The PHACeT Trial. Circ. Res. *117*, 645–654.

42. Oguz, M.M., Oguz, A.D., Sanli, C., and Cevik, A. (2014). Serum levels of soluble ICAM-1 in children with pulmonary artery hypertension. Tex. Heart Inst. J. *41*, 159–164.

43. Sakamaki, F., Kyotani, S., Nagaya, N., Sato, N., Oya, H., Satoh, T., and Nakanishi, N. (2000). Increased plasma P-selectin and decreased thrombomodulin in pulmonary arterial hypertension were improved by continuous prostacyclin therapy. Circulation *102*, 2720–2725.

44. Lapa, M., Acencio, M.M.P., Farias, A.Q., Teixeira, L.R., Fernandes, C.J.C., Jardim, C.P., et al. (2014). Selectins and Platelet-Derived Growth Factor (PDGF) in Schistosomiasis-Associated Pulmonary Hypertension. Lung *192*, 981–986.

45. Stewart, A.O., Bhatia, P.A., McCarty, C.M., Patel, M.V., Staeger, M.A., Arendsen, D.L., Gunawardana, I.W., Melcher, L.M., Zhu, G.-D., Boyd, S.A., et al. (2001). Discovery of inhibitors of cell adhesion molecule expression in human endothelial cells. 1. Selective inhibition of ICAM-1 and E-selectin expression. J. Med. Chem. *44*, 988–1002.

46. Xing, Y., Zhao, S., Wei, Q., Gong, S., Zhao, X., Zhou, F., Ai-Lamki, R., Ortmann, D., Du, M., Pedersen, R., et al. (2018). A novel piperidine identified by stem cell-based screening attenuates pulmonary arterial hypertension by regulating BMP2 and PTGS2 levels. Eur. Respir. J. *51*, 1702229.

47. Charoenphun, P., Meszaros, L.K., Chuamsaamarkkee, K., Sharif-Paghaleh, E., Ballinger, J.R., Ferris, T.J., Went, M.J., Mullen, G.E., and Blower, P.J. (2015). [(89)Zr]oxinate4 for long-term in vivo cell tracking by positron emission tomography. Eur. J. Nucl. Med. Mol. Imaging *42*, 278–287.

48. Li, D., Cheng, S., Zou, S., Zhu, D., Zhu, T., Wang, P., and Zhu, X. (2018). Immuno-PET Imaging of ^{89}Zr Labeled Anti-PD-L1 Domain Antibody. Mol. Pharm. *15*, 1674–1681.